The Astrophysical Journal, 746:23 (12pp), 2012 February 10 doi:10.1088/0004-637X/746/1/23

THE RADIO ACTIVITY–ROTATION RELATION OF ULTRACOOL DWARFS

M. McLean[1], E. Berger[1], and A. Reiners[2]
[1] Harvard-Smithsonian Center for Astrophysics, 60 Garden Street, Cambridge, MA 02138, USA
[2] Institut für Astrophysik, Universität Göttingen, Friedrich-Hund-Platz 1, D-37077 Göttingen, Germany
Received 2011 August 1; accepted 2011 December 22; published 2012 January 20

ABSTRACT

We present a new radio survey of about 100 late-M and L dwarfs undertaken with the Very Large Array. The sample was chosen to explore the role of rotation in the radio activity of ultracool dwarfs. As part of the survey we discovered radio emission from three new objects, 2MASS J 0518113−310153 (M6.5), 2MASS J 0952219−192431 (M7), and 2MASS J 1314203+132001 (M7), and made an additional detection of LP 349-25 (M8). Combining the new sample with results from our previous studies and from the literature, we compile the largest sample to date of ultracool dwarfs with radio observations and measured rotation velocities (167 objects). In the spectral type range M0–M6 we find a radio activity–rotation relation, with saturation at $L_{\rm rad}/L_{\rm bol} \approx 10^{-7.5}$ above $v \sin i \approx 5$ km s^{-1}, similar to the relation in Hα and X-rays. However, at spectral types $\gtrsim$M7 the ratio of radio to bolometric luminosity increases significantly regardless of rotation velocity, and the scatter in radio luminosity increases. In particular, while the most rapid rotators ($v \sin i \gtrsim 20$ km s^{-1}) exhibit "super-saturation" in X-rays and Hα, this effect is not seen in the radio. We also find that ultracool dwarfs with $v \sin i \gtrsim 20$ km s^{-1} have a higher radio detection fraction by about a factor of three compared to objects with $v \sin i \lesssim 10$ km s^{-1}. When measured in terms of the Rossby number (Ro), the radio activity–rotation relation follows a single trend and with no apparent saturation from G to L dwarfs and down to Ro $\sim 10^{-3}$; in X-rays and Hα there is clear saturation at Ro $\lesssim 0.1$, with super-saturation beyond M7. A similar trend is observed for the radio surface flux ($L_{\rm rad}/R_*^2$) as a function of Ro. The continued role of rotation in the overall level of radio activity and in the fraction of active sources, and the single trend of $L_{\rm rad}/L_{\rm bol}$ and $L_{\rm rad}/R_*^2$ as a function of Ro from G to L dwarfs, indicates that rotation effects are important in regulating the topology or strength of magnetic fields in at least some fully convective dwarfs. The fact that not all rapid rotators are detected in the radio provides additional support to the idea of dual dynamo states proposed from spectropolarimetric observations.

Key words: brown dwarfs – radio continuum: stars – stars: activity – stars: low-mass – stars: magnetic field

Online-only material: color figures

1. INTRODUCTION

Rotation plays a key role in the magnetic dynamos of cool stars. The $\alpha\Omega$ dynamo (Parker 1955) is the standard mechanism used to explain magnetic field generation in sun-like stars. The combination of winding of magnetic field lines due to differential rotation and twisting by convective motions results in the generation of a magnetic field whose strength is highly dependent on stellar rotation. Indeed, this dynamo mechanism is supported by the observed correlation between rotation and magnetic activity (indicated by Hα, Ca II *H&K*, X-rays, and radio), as well as between rotation and inferred magnetic field strengths (from Zeeman broadening) in F to early-M dwarfs (Noyes et al. 1984; Stewart et al. 1988; James et al. 2000; Delfosse et al. 1998; Pizzolato et al. 2003; Browning et al. 2010; Reiners et al. 2009; Morin et al. 2010). The critical parameter appears to be the Rossby number, Ro $= P/\tau_c$, where P is the rotation period and τ_c is the convective turnover timescale; magnetic activity increases with a decreasing Rossby number (e.g., Noyes et al. 1984). However, since the $\alpha\Omega$ dynamo operates at the transition layer between the radiative and convective zones in stars where differential rotation is maximized, a separate mechanism may be required to account for magnetic fields in fully convective dwarfs (spectral types $\gtrsim$M3).

Observationally, Hα and X-ray activity measurements demonstrate that the correlation between rotation and activity continues beyond the expected transition to full convection (Delfosse et al. 1998; Mohanty & Basri 2003). However, since the activity in early- to mid-M dwarfs becomes saturated at a fairly low rotation rate, corresponding to $v \approx 5$ km s^{-1}, few objects display the unsaturated correlation. An eventual breakdown in the saturated rotation–activity relation is observed in ultracool dwarfs (spectral type $\gtrsim$M7) in both X-rays and Hα (e.g., Basri & Marcy 1995; Mohanty & Basri 2003; Berger et al. 2008), such that the activity levels decline precipitously in all objects, independent of rotation (e.g., Berger et al. 2010). A similar breakdown is seen in the correlation between rotation and magnetic flux Bf (Reiners & Basri 2010); here B is the magnetic field and f is the magnetic filling factor. Moreover, late-M dwarfs appear to exhibit distinct regimes of magnetic field topologies and strengths with no obvious correlation to the stellar rotation (Morin et al. 2010).

There are also hints of super-saturation among the most rapid rotators (with $v \gtrsim 20$ km s^{-1}) where there appears to be a particularly strong suppression of Hα (Reiners & Basri 2010) and X-ray (James et al. 2000; Berger et al. 2008) activity at spectral types beyond M7. It is unclear whether the super-saturation phenomenon is related to external effects such as centrifugal coronal stripping (Jardine & Unruh 1999; James et al. 2000; Berger et al. 2008), or to the actual generation of the magnetic field. Unfortunately, it is not possible to make direct magnetic flux measurements in rapidly rotating objects because Zeeman broadening is masked by rotational broadening (Morin et al. 2010; Reiners & Basri 2010).

Similarly, there is an inherent difficulty in using Hα and X-ray emission to study field generation in ultracool dwarfs since the decrease in activity may be due to a decoupling

between the increasingly neutral atmosphere and any existing magnetic fields (Mohanty et al. 2002), or to a change in the bulk coronal density (e.g., Berger et al. 2008). This is potentially manifested in the sharp breakdown of the tight radio/X-ray activity correlation (Guedel & Benz 1993; Benz & Guedel 1994) at spectral type M7 (Berger 2002, 2006; Berger et al. 2010). Thus, while X-ray and Hα activity plummet in ultracool dwarfs, the ratio of radio to bolometric luminosity actually increases in the coolest objects, while the radio luminosity itself remains largely unchanged, at least to spectral type ∼L4 (Berger 2002, 2006; Berger et al. 2010). Thus, radio observations indicate that ultracool dwarfs are capable of generating stable large-scale kilo-Gauss magnetic fields. This result has been confirmed with Zeeman broadening observations of M dwarfs (Reiners & Basri 2010), as well as with magnetic topology studies using spectropolarimetry (Zeeman Doppler Imaging (ZDI); Donati et al. 2006; Morin et al. 2010). However, radio activity remains a unique tool for studying the field topology and dissipation in rapid rotators (e.g., Berger et al. 2009; McLean et al. 2011). We note that the determination of magnetic field strength from radio data depends on the details of the dominant emission mechanism (e.g., gyrosynchrotron or electron cyclotron maser; Güdel 2002), but in both cases the radio emission is non-thermal and therefore serves as a proxy for the presence and strength of the magnetic field.

Theoretical studies have led to several proposed models to explain the continued presence of magnetic fields in fully convective stars and brown dwarfs. Durney et al. (1993) proposed a turbulent dynamo that generates small-scale chaotic magnetic fields, with little dependence on rotation. However, this mechanism cannot produce sufficient large-scale magnetic fields to explain the observed Zeeman broadening, or the strong radio activity among ultracool dwarfs, particularly periodic radio emission that appears to require a substantial field with low multipole order (Berger et al. 2009; McLean et al. 2011). Chabrier & Küker (2006) explored the α^2 dynamo, which predicts large-scale primarily toroidal fields with a strong dependence on rotation, and saturation at high rotation rates where the α^2 mode becomes super-critical. This dynamo model has been proposed to dominate among all fast solid-body rotators, even the partially radiative early-M dwarfs. Dobler et al. (2006) conducted three-dimensional hydrodynamic and magnetohydrodynamic (MHD) simulations of fully convective spheres, and found magnetic fields on all spatial scales, as well as differential rotation. They also found that the fields on the largest scales increase with rotation rate, reaching saturation only at fast rotation (Ro $\approx$ 0.01), and exhibiting no sign of super-saturation. The MHD simulations of Browning (2008) also find that faster rotation produces higher magnetic energy densities, as well as magnetic fields on increasingly large scales with a dipolar topology. However, these models do not include the fastest rotators.

In this paper, we study the relation between radio activity and rotation in M and L dwarfs as a way to explore and constrain the magnetic dynamo mechanism of ultracool dwarfs. A radio activity–rotation relation has been found in F–K stars (Stewart et al. 1988; Slee & Stewart 1989), as expected from the X-ray activity–rotation relation and the strong radio/X-ray correlation. Based on a small sample of ultracool dwarfs, Berger et al. (2008) found hints that a connection between radio activity and rotation may persist in late-M and L dwarfs, despite the breakdown in the Hα and X-ray activity–rotation relations. Here we present a much larger sample of objects, taking advantage of new radio observations of 104 M and L dwarfs, as well as new rotation velocity measurements for previously studied objects (Reiners & Basri 2008, 2010). We present the radio observations in Section 2, and new ultracool dwarf detections in Section 3. In Section 4, we study the role of rotation in producing radio activity and discuss implications for dynamo models in Section 5. Our key finding is that the fastest rotators (highest $v \sin i$ and lowest Rossby number) have higher ratios of radio to bolometric luminosity, higher radio surface fluxes, and a higher radio detection fraction, suggesting that rotation continues to play a role in the magnetic dynamo mechanism of ultracool dwarfs.

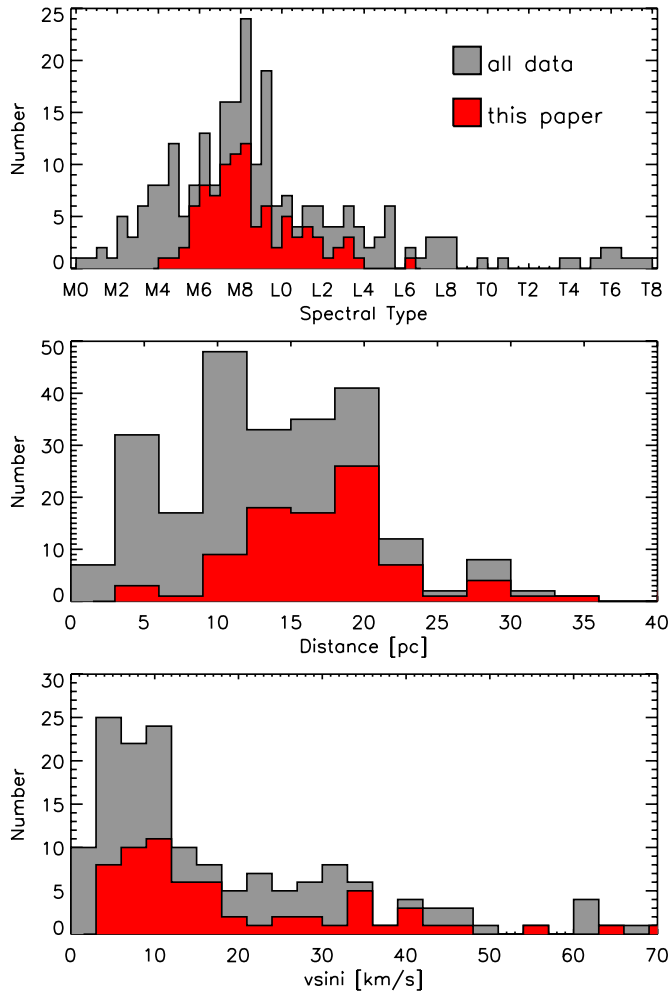

Figure 1. Properties of the survey sources, including spectral types (top), distances (middle), and projected rotation velocities (bottom). The new objects from this survey (Table 1) are shown in red while all data including observations from the literature (Table 2) are shown in gray.

(A color version of this figure is available in the online journal.)

2. OBSERVATIONS

We carried out a survey of 104 M and L dwarfs with the Very Large Array (VLA[3]). The properties of the sources are summarized in Table 1 and plotted in Figure 1. The targets are concentrated in the spectral type range M6–M9, where the X-ray/radio correlation and the X-ray/Hα activity–rotation relation break down. The sample includes sources with no

[3] The VLA is operated by the National Radio Astronomy Observatory, a facility of the National Science Foundation operated under cooperative agreement by Associated Universities, Inc.

Table 1
Results from Our Radio Survey of M and L Dwarfs

2MASS Number	Other Name	Sp.T.	J (mag)	K (mag)	d (pc)	$v \sin i$ (km s^{-1})	$L_{\rm bol}$ ($L_\odot$)	$L_{\rm H\alpha}/L_{\rm bol}$	F_ν (μJy)	$\nu L_\nu/L_{\rm bol}$
0318238−010018	SDSS-MEB-1	M4.0	15.4	14.62	375	...	−1.81	...	<78	<−5.74
0629234−024850A	GJ 234 A	M4.5	6.38	5.49	4	6	−2.89	−3.98	<81	<−8.50
1406493−301828	LHS 2859	M5.0	11.36	10.37	19	...	−2.84	...	<81	<−7.27
2043192+552053	GJ 802 A	M5.0	9.56	8.75	9	6.4	−2.23	...	<93	<−7.03
0004575−170937		M5.5	11.00	10.08	16	...	−3.31	−3.81	<78	<−6.98
1610584−063132	LP 684-33	M5.5	11.35	10.37	18	...	−2.91	...	<96	<−7.19
2132297−051158	LP 698-2	M5.5	11.42	10.38	19	...	−2.91	−5.06	<72	<−7.29
2151270−012713	LP 638-50	M5.5	11.28	10.39	19	...	−2.81	...	<63	<−7.43
2205357−110428	LP 759-25	M5.5	11.66	10.72	19	13	−2.98	−4.20	<84	<−7.15
1236153−310646		M5.5	11.78	10.81	19	...	−3.00	...	<111	<−6.96
0013466−045736	LHS 1042	M6.0	11.46	10.48	17	...	−3.01	...	<81	<−7.23
0024441−270824	GJ 2005 A	M6.0	9.25	8.24	19	9	−3.25	−4.62	<96	<−6.50
1236396−172216		M6.0	11.77	10.63	19	...	−3.02	...	<69	<−7.16
1346460−314925	LP 911-56	M6.0	10.98	10.04	14	...	−2.96	...	<84	<−7.41
1432085+081131	LHS 2935	M6.0	10.11	9.17	9	...	−2.96	...	<81	<−7.79
1552446−262313	LHS 5303	M6.0	10.37	9.30	11	...	−2.98	...	<78	<−7.67
1614252−025100		M6.0	11.30	10.28	18	...	−2.87	−4.19	<90	<−7.23
2049527−171608		M6.0	11.81	10.81	19	...	−3.02	...	<60	<−7.22
0518113−310153		M6.5	11.88	10.90	20	...	−3.04	...	181 ± 27	−6.73
0931223−171742	LP 788-1	M6.5	11.07	10.07	13	...	−3.09	...	<54	<−7.55
1516407+391048	LP 222-65	M6.5	10.80	9.81	12	...	−3.23	...	<81	<−7.30
1606339+405421	LHS 3154	M6.5	11.05	10.07	12	...	−3.34	...	<117	<−7.02
1646315+343455	LHS 3241	M6.5	10.53	9.61	11	...	−3.15	...	<84	<−7.46
0535218−054608AB		M6.5	14.65	13.47	156	...	−2.35	...	<93	<−5.88
0711113+432959	LHS 1901	M6.5	9.98	9.13	13	...	−2.94	...	<117	<−7.35
0741068+173845	LHS 1937	M7.0	12.01	10.94	18	10	−3.17	−4.10	<75	<−7.03
0818580+233352		M7.0	12.18	11.15	19	4.5	−3.19	−4.11	<78	<−6.94
0952219−192431		M7.0	11.87	10.87	30	6	−3.08	−3.94	<69	<−6.43
									233 ± 15	−6.20
1048126−112009	GJ 3622	M7.0	8.86	7.93	5	<3	−3.09	−4.63	<96	<−8.20
1141440−223215		M7.0	12.63	11.57	22	10	−3.25	−4.90	<108	<−6.62
1314203+132001A		M7.0	9.75	8.79	16	45	−3.17	−3.97	1156 ± 15	−5.92
1354087+084608		M7.0	12.19	11.16	17	...	−3.79	...	<105	<−6.31
1356414+434258	LP 220-13	M7.0	11.71	10.65	16	14	−3.59	−3.92	<99	<−6.61
1534570−141848	2MUCD 11346	M7.0	11.38	10.31	11	10	−3.34	−4.01	<87	<−7.21
2337383−125027	LP 763-3	M7.0	11.46	10.45	19	...	−2.89	−3.50	<84	<−7.20
0351000−005244	GJ 3252	M7.5	11.30	10.23	15	6.5	−3.06	−4.16	<123	<−7.10
1006319−165326	LP 789-23	M7.5	12.04	10.99	16	16	−3.28	−4.22	<87	<−6.96
1155429−222458	LP 851-346	M7.5	10.94	9.88	10	33	−3.30	−4.58	<90	<−7.36
1246517+314811	LHS 2632	M7.5	12.23	11.21	18	7.3	−3.25	−5.27	<90	<−6.86
1250526−212113		M7.5	11.16	10.13	11	...	−3.25	...	<72	<−7.39
1253124+403403	LP 218-8	M7.5	12.19	11.16	17	9	−3.29	−4.27	<78	<−6.94
1332244−044112		M7.5	12.37	11.28	21	9	−3.18	−4.37	<60	<−6.97
1507277−200043		M7.5	11.71	10.66	14	64	−3.61	−4.47	<96	<−6.69
1546054+374946		M7.5	12.44	11.41	20	10	−3.25	−3.98	<84	<−7.04
1757154+704201	LP 44-162	M7.5	11.45	10.40	12	33	−3.30	−5.01	<117	<−7.05
2331217−274950		M7.5	11.30	10.23	15	9	−3.06	−4.03	<72	<−7.32
0027559+221932	LP 349-25 B	M8.0	10.61	9.57	10	56	−3.12	−4.53	323 ± 14	−6.95
0248410−165121		M8.0	12.55	11.42	17	<3	−3.45	−4.25	<81	<−6.77
0320596+185423	LP 412-31	M8.0	11.76	10.64	15	15	−3.26	−3.87	<81	<−7.08
0544115−243301		M8.0	12.53	11.46	19	<3	−3.33	−4.12	<63	<−6.90
0629235−024851B	GJ 234 B	M8.0	8.38	7.33	4	...	−3.00	...	<81	<−8.45
1016347+275149	LHS 2243	M8.0	11.99	10.96	14	<3	−3.38	−3.87	<84	<−6.99
1024099+181553	2MUCD 10906	M8.0	12.28	11.24	16	5	−3.38	−4.84	<87	<−6.86
1309218−233035		M8.0	11.79	10.67	13	7	−3.63	−4.35	<93	<−6.74
1428041+135613	LHS 2919	M8.0	11.01	10.03	10	...	−3.37	...	<90	<−7.25
1440229+133923		M8.0	12.40	11.34	18	<3	−3.33	−4.60	<75	<−6.87
1444171+300214	LP 326-21	M8.0	11.67	10.62	13	...	−3.61	...	<81	<−6.87
1843221+404021	GJ 4073	M8.0	11.31	10.31	14	5	−3.09	−4.11	<96	<−7.21
2206227−204706		M8.0	12.37	11.32	27	24	−2.95	−4.54	<84	<−6.83
2349489+122438	LP 523-55	M8.0	12.60	11.56	20	4	−3.31	−4.61	<60	<−6.89
2351504−253736A		M8.0	12.47	11.27	18	36	−3.36	−4.61	<69	<−6.88
1121492−131308	GJ 3655	M8.5	11.93	10.74	12	27	−3.68	−3.87	<102	<−6.74
1124048+380805		M8.5	12.71	11.57	19	7.5	−3.41	−5.16	<66	<−6.80
1403223+300754		M8.5	12.68	11.60	19	10	−3.39	−4.49	<60	<−6.86

Table 1
(Continued)

2MASS Number	Other Name	Sp.T.	J (mag)	K (mag)	d (pc)	$v \sin i$ (km s^{-1})	$L_{\rm bol}$ ($L_\odot$)	$L_{\rm H\alpha}/L_{\rm bol}$	F_ν (μJy)	$\nu L_\nu/L_{\rm bol}$
2353594−083331		M8.5	13.03	11.93	22	4.5	−3.41	−4.42	<69	<−6.64
0443376+000205		M9.0	12.51	11.22	16	13.5	−3.47	−5.00	<54	<−6.99
1224522−123835		M9.0	12.57	11.35	17	7	−3.94	−4.52	<102	<−6.20
1411213−211950		M9.0	12.44	11.33	16	44	−3.93	−4.93	<93	<−6.29
1428432+331039	LHS 2924	M9.0	11.99	10.74	11	11	−3.59	−5.14	<84	<−6.98
1707234−055824	2MUCD 20701	M9.0	12.25	10.90	17	...	−3.31	...	<81	<−6.92
2200020−303832AB		M9.0	13.44	12.20	35	17	−3.17	−5.03	<78	<−6.44
0024246−015819	BRI B0021-02	M9.5	11.99	10.54	12	33	−3.45	−6.12	<60	<−7.09
1438082+640836		M9.5	12.99	11.65	18	12	−4.08	−4.77	<105	<−5.96
2237325+392239	G216-7B	M9.5	13.34	12.18	19	...	−3.66	−5.02	<81	<−6.46
0314034+160305		L0.0	12.53	11.24	14	19	−3.59	−4.69	<108	<−6.66
1159385+005726		L0.0	14.08	12.81	30	71	−3.57	−5.06	<54	<−6.35
1221277+025719		L0.0	13.17	11.95	19	25	−3.59	−4.88	<78	<−6.54
1731297+272123		L0.0	12.09	10.91	12	15	−3.56	−4.80	<69	<−7.03
1854459+842947		L0.0	13.66	12.47	23	7	−3.62	−4.73	<87	<−6.29
1412244+163311		L0.5	13.89	12.52	25	19	−3.61	−5.50	<69	<−6.33
1441371−094559		L0.5	14.02	12.66	28	23	−3.59	−5.48	<84	<−6.20
2351504−253736B		L0.5	12.47	11.27	18	41	−3.36	−5.22	<69	<−6.87
0235599−233120		L1.0	13.67	12.19	21	13	−3.63	−6.44	<99	<−6.30
1045240−014957		L1.0	13.16	11.78	17	<3	−3.65	−6.44	<57	<−6.71
1048428+011158		L1.0	12.92	11.62	15	17	−3.69	−5.71	<21	<−7.22
1439283+192914		L1.0	12.76	11.55	14	11	−3.67	−5.20	<78	<−6.71
1555157−095605		L1.0	12.56	11.44	13	11	−3.68	−5.35	<84	<−6.75
1145571+231729	GL Leo	L1.5	15.39	13.95	44	14	−3.70	−5.27	<90	<−5.65
1334062+194035		L1.5	15.48	14.00	46	30	−3.68	−6.53	<60	<−5.74
1645221−131951		L1.5	12.45	11.15	12	9	−3.69	−5.66	<108	<−6.71
1807159+501531	2MUCD 11756	L1.5	12.93	11.62	15	76	−3.71	−5.26	<84	<−6.62
0828341−130919		L2.0	12.80	11.30	14	33	−3.64	−6.63	<66	<−6.83
0921141−210444	DENIS-092114	L2.0	12.78	11.69	12	15	−3.83	<−6.42	<75	<−6.72
1029216+162652		L2.5	14.29	12.62	23	29	−3.72	−5.76	<33	<−6.64
1047310−181557		L2.5	14.20	12.89	22	15	−3.86	−5.99	<63	<−6.23
0913032+184150		L3.0	15.97	14.28	46	34	−3.77	−6.86	<102	<−5.47
1203581+001550		L3.0	14.01	12.48	19	39	−3.84	−6.02	<63	<−6.39
1506544+132106		L3.0	13.37	11.74	14	20	−3.80	−6.32	<78	<−6.60
1615441+355900		L3.0	14.54	12.94	24	13	−3.82	<−5.98	<75	<−6.13
1707234−055824	2MUCD 20701	L3.0	13.96	12.25	17	...	−3.80	...	<81	<−6.42
0700366+315726A		L3.5	13.23	11.62	12	41	−3.88	−6.04	<78	<−6.39

Notes. Properties of the M and L dwarfs observed in this paper. The columns are (left to right) (1) 2MASS number; (2) other name; (3) spectral type; (4) J-band magnitude; (5) K-band magnitude; (6) distance from parallax or photometric estimate (from SIMBAD; Faherty et al. 2009; Cruz et al. 2003); (7) projected rotation velocity (from Mohanty & Basri 2003; Reid et al. 2002; Reiners & Basri 2008, 2010; Jenkins et al. 2009); (8) bolometric luminosity; (9) Hα activity (from Delfosse et al. 1998; Mohanty & Basri 2003; Reiners & Basri 2008, 2010); (10) radio density flux; and (11) ratio of radio to bolometric luminosity.

previous radio observations, as well as several objects with previous detections or upper limits. The majority of the sample is located at $\lesssim$20 pc. Taking into account objects with new velocity measurements that were observed in previous radio surveys, we have increased the number of objects with both radio and rotation measurements by about a factor of three compared to previous studies.

Each object was observed for a single contiguous hour at 8.46 GHz using the standard continuum mode with 2 × 50 MHz contiguous bands. The flux density scale was determined using the extragalactic calibrators 3C 48 (J 0137+331), 3C 138 (J 0521+166), or 3C 286 (J 1331+305), while the phase was monitored using calibrators located within 10° of the target sources. The data were reduced and analyzed using the Astronomical Image Processing System. The resulting flux density measurements are given in Table 1.

Previous radio observations collected from the literature are presented in Table 2 (Jackson et al. 1989; White et al. 1989; Guedel et al. 1993; Krishnamurthi et al. 1999; Berger et al. 2001, 2009; Berger 2002, 2006; Burgasser & Putman 2005; Phan-Bao et al. 2007). We note that some of the data from previous surveys were obtained at a frequency of 4.9 GHz, accounting for about 10% of the total sample in this paper. Multi-frequency observations of individual ultracool dwarfs point to a range of spectral indices between 4.9 and 8.5 GHz, from $\beta \sim 2$ to ~ -2 ($F_\nu \propto \nu^\beta$; e.g., Berger et al. 2001; McLean et al. 2011; Ravi et al. 2011). These are typical of broadband gyrosynchrotron emission in the optically thick and thin regime, respectively, suggesting that the peak of the radio spectral energy distribution is generally in the range of a few GHz, well matched to our study. The scatter resulting from the uncertainty in the spectral index is smaller than the observed range of radio luminosities at a fixed spectral type or rotation velocity, and therefore it has no significant effect on the trends discussed in this paper (particularly since only 10% of the data were obtained at 4.9 GHz).

We note that in some extreme cases narrowband emission, which is likely due to a coherent process, may lead to an

Table 2
Results from the Literature

2MASS Number	Other Name	Sp.T.	J (mag)	K (mag)	d (pc)	$v \sin i$ (km s^{-1})	$L_{\rm bol}$ ($L_\odot$)	$L_{\rm H\alpha}/L_{\rm bol}$	F_ν (μJy)	$\nu L_\nu/L_{\rm bol}$	Ref.
0459348+014700	GJ 182	M0.0	7.12	6.26	26	...	−1.11	...	307	−8.14	1
1120052+655047	GJ 424	M0.0	6.31	5.53	9	...	−1.11	<−5.0	<240	<−8.33	2
1300466+122232	GJ 494B	M0.5	6.44	5.58	11	10	−1.63	...	<115	<−8.53	1
0042482+353255	GL 29.1	M1.0	7.16	6.32	24	...	−1.27	...	<150	<−8.14	3
0610346−215152	GJ 229A	M1.0	5.10	4.17	6	1	−1.74	...	<290	<−8.61	2
0734374+315209	GJ 278C	M1.0	6.07	5.24	15	...	−1.21	...	268	−8.58	1
0102389+622042	GL 49	M1.5	6.23	5.37	10	<3.4	−1.66	...	<370	<−8.10	2
0018225+440122	GL 15A	M2.0	5.25	4.02	4	2.9	−2.37	...	<220	<−8.52	2
1103202+355811	GJ 411	M2.0	4.20	3.25	3	<2.9	−2.10	<−5.0	<168	<−9.61	4
1105290+433135	GJ 412A	M2.0	5.54	4.77	5	<3.0	−1.95	<−5.0	<220	<−8.68	2
2238455−203716	GJ 867A	M2.0	5.67	4.80	9	...	−1.58	...	360	−8.53	1
2349125+022403	GJ 908	M2.0	5.83	5.04	6	<3.1	−1.90	<−5.0	<200	<−8.59	2
0533448+015643	GJ 207.1	M2.5	7.76	6.86	17	10	−1.86	...	<150	<−7.85	3
1332446+164839	GJ 516A	M2.5	7.64	6.83	20	...	−1.25	...	<320	<−8.10	2
1454292+160603	GJ 569AB	M2.5	6.63	5.77	10	<2.5	−1.84	...	<390	<−7.92	2
0032297+671404	GL 22B	M3.0	7.17	6.38	10	...	−1.97	...	<390	<−7.77	2
1332446+164839	GJ 516B	M3.0	7.64	6.83	14	...	−1.91	...	<320	<−7.65	2
1655528−082010	GJ 644A	M3.0	5.27	4.40	7	...	−1.66	...	890	−8.52	5
1842466+593749	GL 725A	M3.0	5.19	4.43	4	<5	−2.06	<−5.0	<180	<−8.92	3
1849492−235010	GJ 729	M3.0	6.22	5.37	3	4	−2.71	...	165	−9.70	1
1855274+082409	GJ 735	M3.0	6.31	5.43	12	<10	−1.58	...	450	−7.98	3
0004364−404402	GJ 1001A	M3.5	8.60	7.74	10	...	−2.66	...	<45	<−8.31	6
0032297+671408	GL 22A	M3.5	6.84	6.04	10	...	−1.85	...	<390	<−7.89	2
0532146+094915	GJ 206	M3.5	7.42	6.56	13	10	−1.93	...	163	−8.52	1
1736259+682022	GJ 687	M3.5	5.34	4.55	5	<5	−1.94	<−5.0	300	−9.15	2
1842468+593737	GL 725B	M3.5	5.72	5.00	4	<7	−2.25	<−5.0	<180	<−8.74	3
1916552+051008	GJ 752A	M3.5	5.58	4.67	6	<2.6	−1.90	<−5.0	<290	<−8.44	2
2238453−203651	GJ 867B	M3.5	7.34	6.49	9	...	−2.23	...	810	−7.33	2
2331520+195614	GJ 896A	M3.5	6.16	5.33	6	10	−2.02	...	460	−8.34	1
0112305−165957	GL 54.1	M4.0	7.26	6.42	4	<2.5	−2.92	...	<390	<−7.69	2
0139011−175701	GL 65A	M4.0	6.28	5.34	3	29.4	−2.89	...	1650	−7.51	1
0431114+585837	GJ 169.1AB	M4.0	6.62	5.72	6	1.9	−2.35	−5.16	<230	<−8.12	4
1147444+004816	GJ 447	M4.0	6.51	5.65	3	<2	−2.73	<−5	<210	<−8.24	2
1233163+090126	GJ 473A	M4.0	6.88	6.04	4	...	−2.75	...	200	−7.92	2
2227595+574145	GJ 860B	M4.0	5.58	4.78	4	4.7	−2.15	−4.11	12830	−7.35	2
0200127+130311	GL 83.1	M4.5	7.51	6.65	5	3.8	−2.87	−4.35	<260	<−7.75	2
0415217−073917	GJ 166C	M4.5	6.75	5.96	5	5	−2.41	−3.95	310	<−8.28	1
0629234−024850	GJ 234A	M4.5	6.38	5.49	4	6	−2.89	−3.98	550	−7.98	2
0710018+383145	GJ 268	M4.5	6.73	5.85	6	...	−2.27	...	<330	<−8.04	2
0744401+033308	GJ 285	M4.5	6.58	5.70	6	6.5	−2.27	−3.18	320	−8.24	1
1019363+195212	GJ 388	M4.5	5.45	4.59	5	2.7	−2.01	−3.77	250	−9.00	1
1300335+054108	GJ 493.1	M4.5	8.55	7.66	8	16.8	−2.80	−3.96	1280	−7.09	2
1634204+570943	GJ 630.1A	M4.5	8.50	7.80	15	27.5	−2.10	...	<530	<−7.18	7
1719529+263002	GJ 669B	M4.5	8.23	7.35	12	<10	−2.32	...	510	−7.15	2
2029483+094120	GJ 791.2	M4.5	8.23	7.31	10	...	−2.74	−3.84	<350	<−7.10	2
2246498+442003	GJ 873A	M4.5	6.11	5.30	5	6.9	−2.17	−3.70	<300	<−8.28	2
0103197+622155	GL 51	M5.0	8.61	7.72	10	...	−2.60	...	7280	−5.83	2
2217189−084812	GJ 852A	M5.0	9.02	8.17	10	...	−2.97	...	<290	<−6.87	2
2217187−084818	GJ 852B	M5.0	9.46	8.53	9	32	−2.61	...	<290	<−7.28	2
1953544+442454	GJ 1245A	M5.5	7.79	6.85	5	22.5	−3.01	−4.27	<310	<−7.50	4
1953550+442455	GJ 1245B	M5.5	8.28	7.39	5	6.8	−3.14	−4.25	<310	<−7.34	4
0018254+440137	GL 15B	M6.0	6.79	5.95	4	<3.1	−2.77	...	<220	<−8.12	2
0024441−270825	GJ 2005A	M6.0	9.25	8.24	7	9	−3.25	−4.62	161 ± 15	−7.39	6
1105313+433117	GJ 412B	M6.0	8.74	7.84	5	7.7	−3.33	−3.95	<220	<−7.30	2
1056288+070052	GJ 406	M6.5	7.09	6.08	2	<3	−3.37	−3.89	<390	<−7.63	2
0435161−160657	LP 775-31	M7.0	10.4	9.34	9	...	−3.59	−4.28	<48	<−7.44	6
0440232−053008	LP 655-48	M7.0	10.68	9.56	10	16.5	−3.62	−3.80	<39	<−7.39	6
0752239+161215	LP 423-31	M7.0	10.83	9.82	11	9	−3.56	−3.44	<39	<−7.39	6
1456383−280947	GJ 3877	M7.0	9.96	8.92	7	8	−3.29	−4.02	270 ± 40	−7.23	8
1634216+571008	GJ 630.1B	M7.0	14.11	14.14	16	...	−3.13	...	<530	<−6.05	7
1655352−082340	VB 8	M7.0	9.78	8.83	6	9	−3.21	...	<24	<−8.37	9
0148386−302439		M7.5	12.28	11.24	18	48	−3.67	−4.35	<45	<−6.73	6
0331302−304238	LP 888-18	M7.5	11.37	10.28	12	<3	−3.70	−4.07	<72	<−6.86	6
0417374−080000		M7.5	12.17	11.05	17	7	−3.72	−4.32	<36	<−6.83	6

Table 2
(Continued)

2MASS Number	Other Name	Sp.T.	J (mag)	K (mag)	d (pc)	$v \sin i$ (km s^{-1})	$L_{\rm bol}$ ($L_\odot$)	$L_{\rm H\alpha}/L_{\rm bol}$	F_ν (μJy)	$\nu L_\nu/L_{\rm bol}$	Ref.
0429184−312356		M7.5	10.89	9.80	10	<3	−3.70	−3.93	<48	<−7.23	6
1521010+505323	NLTT 40026	M7.5	12.00	10.92	16	40	−3.70	−4.88	<39	<−6.88	6
0019262+461407		M8.0	12.61	11.47	19	68	−3.80	−4.51	<33	<−6.68	6
0350573+181806	LP 413-53	M8.0	12.95	11.76	23	4	−3.82	...	<105	<−6.02	6
0436103+225956		M8.0	13.76	12.19	140	...	−2.62	...	<45	<−6.02	6
0517376−334902		M8.0	12.00	10.82	15	8	−3.82	−4.42	<54	<−6.70	6
1016347+275149	LHS 2243	M8.0	11.95	10.95	16	<3	−3.65	−3.87	<45	<−6.88	10
1048146−395606	DENIS 1048	M8.0	9.55	8.45	4	18	−3.39	−5.15	140 ± 40	−7.83	8
									29600 ± 100	−5.51	8
1139511−315921		M8.0	12.67	11.49	20	...	−3.39	...	<99	<−6.60	8
1534570−141848		M8.0	11.39	10.31	11	10	−3.39	−4.01	<111	<−7.06	8
1843221+404021	GJ 4073	M8.0	11.30	10.27	14	5	−3.51	−4.11	<48	<−7.10	6
1916576+050902	VB 10	M8.0	9.95	8.81	6	6.5	−3.35	<−5	<81	<−7.81	9
2037071−113756		M8.0	12.28	11.26	17	<3	−3.74	−5.02	<33	<−6.87	6
0335020+234235		M8.5	12.26	11.26	19	...	−3.61	...	<69	<−6.57	6
1454290+160605	GJ 569Ba	M8.5	11.14	10.02	10	...	−3.80	...	<30	<−7.32	6
1501081+225002	TVLM 513-465	M8.5	11.80	10.74	11	60	−3.59	...	190 ± 15	−6.66	10
									980 ± 40	−5.95	10
1835379+325954	LSR J1835+3	M8.5	10.27	9.15	6	44	−3.93	−4.85	525 ± 15	−6.42	6
0140026+270150		M8.5	12.49	11.43	19	6.5	−3.32	...	<20	<−6.93	11
0019457+521317		M9.0	12.82	11.62	19	9	−3.95	−4.29	<42	<−6.47	6
0109511−034326	LP 647-13	M9.0	11.70	10.42	11	13	−3.98	−4.50	<33	<−7.00	6
0339352−352544	LP 944-20	M9.0	10.75	9.52	5	26	−3.79	−5.30	74 ± 13	−7.53	12
									2600 ± 200	−5.99	12
0434152+225031		M9.0	13.74	11.87	140	...	−2.53	...	<69	<−5.92	6
0436389+225812		M9.0	13.70	12.34	140	...	−2.59	...	<57	<−5.95	6
0537259−023432		M9.0	18.22	17.00	352	...	−3.56	...	<66	<−4.11	6
0810586+142039		M9.0	12.77	11.59	20	11	−3.39	...	<39	<−6.52	11
0853362−032932	GJ 3517	M9.0	11.18	9.97	9	13.5	−3.49	−3.93	<81	<−7.33	10
1454280+160605	GJ 569Bb	M9.0	11.65	10.43	10	...	−4.04	...	<30	<−7.08	6
1627279+810507		M9.0	13.03	11.88	21	...	−3.45	...	<60	<−6.23	11
1707183+643933		M9.0	12.54	11.38	17	...	−3.44	...	<60	<−6.43	11
1707234−055824		M9.0	12.06	10.71	15	...	−3.87	...	<48	<−6.68	6
0024246−015819	BRI B0021-0	M9.5	11.99	10.54	12	33	−3.50	−6.12	83 ± 18	−7.18	10
0027420+050341	PC 0025+044	M9.5	16.08	14.87	72	13	−3.62	−3.39	<75	<−5.37	10
0109217+294925		M9.5	12.91	11.68	19	7	−3.49	...	<54	<−6.33	11
0149089+295613		M9.5	13.45	11.98	17	12	−3.74	...	<140	<−5.76	11
0345431+254023		L0.0	13.92	12.67	27	...	−3.56	...	<87	<−6.22	10
0746425+200032		L0.5	11.78	10.47	12	31	−3.93	−5.29	224 ± 15	−6.38	13
									15000 ± 100	−4.55	13
1421314+182740		L0.0	13.23	11.94	20	...	−3.56	...	<42	<−6.32	11
0602304+391059	LSR 0602+39	L1.0	12.30	10.86	11	9	−4.28	−6.05	<30	<−6.78	6
1300425+191235		L1.0	12.72	11.62	14	10	−4.12	−5.71	<87	<−6.23	6
0213288+444445		L1.5	13.49	12.21	19	...	−4.24	...	<30	<−6.32	6
1807159+501531		L1.5	12.93	11.60	15	76	−4.24	−5.26	<39	<−6.42	6
2057540−025230		L1.5	13.12	11.72	16	62	−4.23	−4.92	<36	<−6.37	6
0109015−510049		L2.0	12.23	11.09	10	...	−3.89	...	<111	<−6.65	8
0445538−304820		L2.0	13.41	11.98	17	...	−4.33	...	<66	<−5.99	6
1305401−254110	Kelu-1	L2.0	13.41	11.75	19	60	−3.57	−5.69	<27	<−7.04	9
0523382−140302		L2.5	13.08	11.64	13	21	−4.39	−6.52	<39	<−6.61	6
									231 ± 14	−5.84	6
0251149−035245		L3.0	13.06	11.66	12	...	−4.42	...	<36	<−6.12	6
1721039+334416		L3.0	13.62	12.49	15	...	−4.46	...	<48	<−6.32	6
2104149−103736		L3.0	13.84	12.37	17	27	−4.47	−5.97	<24	<−6.26	6
0036161+182110		L3.5	12.47	11.06	9	45	−4.51	−6.26	134 ± 16	−6.06	10
									720 ± 40	−5.33	10
0045214+163444		L3.5	13.06	11.37	10	...	−4.58	...	<39	<−6.41	6
1424390+091710		L4.0	15.69	14.17	32	...	−4.04	...	<96	<−5.56	10
1705483−051646		L4.0	13.31	12.03	11	26	−4.65	−7.12	<45	<−6.22	6
0141032+180450		L4.5	13.88	12.49	13	...	−4.76	...	<30	<−6.15	6
0652307+471034		L4.5	13.54	11.69	11	...	−4.66	...	<33	<−6.31	6
2224438−015852		L4.5	14.07	12.02	11	32	−4.76	−6.48	<33	<−6.19	6
0004348−404405	GJ 1001BC	L5.0	13.11	11.40	10	42	−4.67	−7.42	<45	<−6.30	6
0144353−071614		L5.0	14.19	12.27	13	...	−4.73	...	<33	<−6.08	6

Table 2
(Continued)

2MASS Number	Other Name	Sp.T.	J (mag)	K (mag)	d (pc)	$v \sin i$ (km s^{-1})	$L_{\rm bol}$ ($L_\odot$)	$L_{\rm H\alpha}/L_{\rm bol}$	F_ν (μJy)	$\nu L_\nu/L_{\rm bol}$	Ref.
0205034+125142		L5.0	15.68	13.67	27	...	−4.67	...	<48	<−5.37	6
0835425−081923		L5.0	13.17	11.14	9	23	−4.60	−7.42	<30	<−6.58	6
1228152−154734		L5.0	14.38	12.77	20	22	−4.19	...	<87	<−5.84	10
1507476−162738		L5.0	12.82	11.31	7	32	−4.23	−8.18	<57	<−6.87	10
1515008+484741		L6.0	14.06	12.56	9	...	−5.11	...	<27	<−6.12	6
0439010−235308		L6.5	14.41	12.82	11	...	−5.10	...	<42	<−5.79	6
0030300−145033		L7.0	16.28	14.48	27	...	−5.01	...	<57	<−4.96	6
0205294−115929		L7.0	14.59	13.00	20	22	−4.65	...	<30	<−5.87	6
1728114+394859		L7.0	15.99	13.91	24	...	−4.86	...	<54	<−5.23	6
0423485−041403		L7.5	14.46	12.93	15	...	−4.83	...	<42	<−5.77	6
0825196+211552		L7.5	15.10	13.03	11	19	−5.21	−8.18	<45	<−5.66	6
2252107−173013		L7.5	14.31	12.90	8	...	−5.29	...	<30	<−5.98	6
0929336+342952		L8.0	16.60	14.64	22	...	−5.25	...	<42	<−5.03	6
1523226+301456		L8.0	16.06	14.35	19	...	−5.27	...	<45	<−5.12	6
1632291+190441		L8.0	15.87	14.00	15	30	−5.31	...	<54	<−5.17	6
0151415+124430		T0.0	16.57	15.18	21	...	−5.37	...	<51	<−4.84	6
2204105−564657A		T1.0	12.29	11.35	4	...	−5.03	...	<72	<−6.58	6
0207428+000056		T4.0	16.80	15.41	29	...	−5.21	...	<39	<−4.87	6
0559191−140448		T4.5	13.80	13.58	10	...	−4.53	...	<27	<−6.60	6
1534498−295227		T5.5	14.90	14.84	14	...	−5.00	...	<63	<−5.52	6
1624144+002916		T6.0	15.49	15.52	11	...	−5.16	...	<36	<−5.78	6
2204105−564657B		T6.0	13.23	13.53	4	...	−5.03	...	<72	<−6.58	6
1047539+212423		T6.5	15.82	16.41	11	...	−5.35	...	<45	<−6.26	6
1346464−003150		T6.5	16.00	15.77	15	...	−5.00	...	<105	<−5.23	10
0610351−215117	GJ 229B	T7.0	14.20	14.30	6	...	−5.21	...	<69	<−6.01	9
1217111−031113		T7.5	15.86	15.89	11	...	−5.32	...	<111	<−5.13	6
0415195−093506		T8.0	15.70	15.43	6	...	−5.73	...	<45	<−5.68	6

Notes. Properties of the M, L, and T dwarfs from the literature. The columns are (left to right) (1) 2MASS number; (2) other name; (3) spectral type; (4) J-band magnitude; (5) K-band magnitude; (6) distance from parallax or photometric estimate (from SIMBAD; Faherty et al. 2009; Cruz et al. 2003); (7) projected rotation velocity (from Mohanty & Basri 2003; Reid et al. 2002; Reiners & Basri 2008, 2010; Jenkins et al. 2009); (8) bolometric luminosity; (9) Hα activity (from Delfosse et al. 1998; Mohanty & Basri 2003; Reiners & Basri 2008, 2010); (10) radio density flux; (11) ratio of radio to bolometric luminosity; and (12) references for radio flux density measurements.

References. (1) Guedel et al. 1993; (2) White et al. 1989 (5 GHz); (3) Willson et al. 1988 (5 GHz); (4) Bower et al. 2009 (5 GHz); (5) Jackson et al. 1989; (6) Berger 2006; (7) Caillault et al. 1988 (5 GHz); (8) Burgasser & Putman 2005; (9) Krishnamurthi et al. 1999; (10) Berger 2002; (11) Phan-Bao et al. 2007; (12) Berger et al. 2001; (13) Berger et al. 2009.

unusually large ratio between different frequencies (e.g., Hallinan et al. 2008; Berger et al. 2009). However, these cases are rare and we do not have sufficient information at the present to determine the effect at different frequencies. Thus, the presence of narrowband emission may also lead to some increase in the scatter, but it will not significantly affect the trends discussed in this paper.

3. NEW RADIO DETECTIONS

As part of this new survey we detect radio emission from four objects: 2MASS J 0518113 − 310153 (M6.5), 2MASS J 0952219 − 192431 (M7), 2MASS J 1314203 + 1320011 (M7; McLean et al. 2011), and the previously detected binary system LP 349-25 (M8; Phan-Bao et al. 2007). The measured flux densities are 181 ± 27 μJy, 233 ± 15μJy, 1156 ± 15 μJy, and 323 ± 14 μJy, respectively. The fractional circular polarizations for the four objects are $f_c \lesssim 45\%$ (2M 0518 − 3101), $f_c \lesssim 30\%$ (2M 0952 − 1924), $f_c = 18 \pm 2\%$ (2M 1314 + 1320), and $f_c \lesssim 23\%$ (LP 349-25). These values are consistent with the level of circular polarization in the quiescent emission observed in other ultracool dwarfs (e.g., Berger 2002, 2006). The flux density measured for LP 349-25 is consistent with the value reported by Phan-Bao et al. (2007). No radio emission was detected from GJ 2005, BRI 0021-0214, or GJ 234A, despite previous radio detections (White et al. 1989; Berger 2002, 2006). Our upper limits for GJ 2005 and BRI 0021-0214 are only a factor of 1.7 and 1.4 below the previous detections, respectively. However, the upper limit on GJ 234A is almost seven times below the detection from White et al. (1989), indicative of long-term variability.

We also carried out a 10 hr follow-up observation of 2M 0952 − 1924 at 4.96 GHz and 8.46 GHz, but found no significant detection, to a limit of 69 μJy, a factor of 2.4 below the original detection. This indicates that the initial detection was either a flare, or that the source experiences long-term variability. Since 2M 0952 − 1924 has a rotation velocity of $v \sin i \approx 6$ km s^{-1}, its rotation period could be as long as 20 hr, indicating that the non-detection in 10 hr could also result from significant rotational modulation (Berger et al. 2005, 2009; Hallinan et al. 2006, 2007; McLean et al. 2011).

4. EXPLORING THE ROLE OF ROTATION

To explore the connection between rotation and radio activity we study the full sample of M and L dwarfs with radio observations and measured rotation velocities. In Figure 2, we plot the ratio of radio to bolometric luminosity as a function of spectral type for the full sample (Tables 1 and 2). Bolometric luminosities are derived using the following bolometric correction factors: (1) for the M dwarfs we use the mean of $BC_J = 2.43 + 0.0895(SP)$ and $BC_K = 1.53 + 0.148(SP) - 0.0105(SP)^2$,

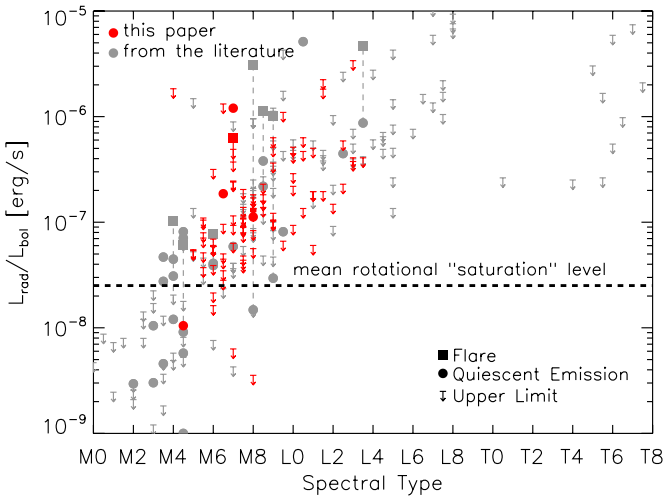

Figure 2. Ratio of radio to bolometric luminosity as a function of spectral type. Shown are flares (squares), quiescent emission (circles), and upper limits (arrows). Red symbols represent the objects from this survey (Table 1) while gray symbols represent objects from the literature (Table 2). The mean rotationally saturated level of emission for early- to mid-M dwarfs is shown as a dashed line (see Figure 5). The clear trend of increased L_{rad}/L_{bol} as a function of later spectral type is seen in the ultracool dwarfs.

(A color version of this figure is available in the online journal.)

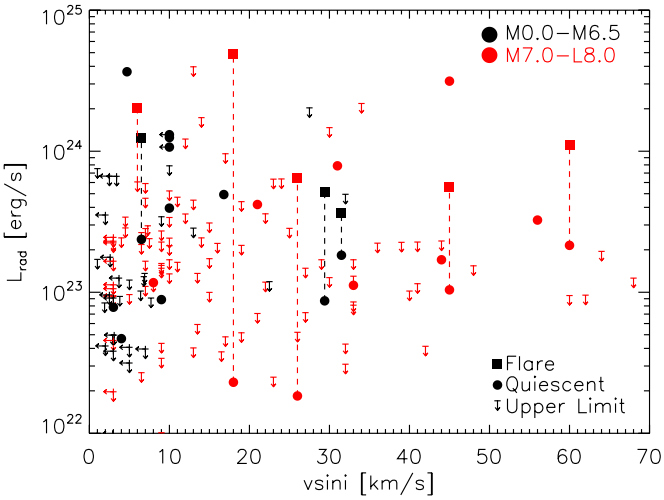

Figure 4. Radio luminosity as a function of projected rotation velocity. Shown are flares (squares), quiescent emission (circles), and radio upper limits (arrows). Left arrows indicate upper limits in $v \sin i$. Red symbols represent objects later than M7, while black symbols represent objects with spectral types M0–M6.5. No obvious trend is detected, but there is a tantalizing paucity of objects with radio luminosity of $\lesssim 10^{23}$ erg s^{-1} at $v \sin i \gtrsim 30$ km s^{-1}.

(A color version of this figure is available in the online journal.)

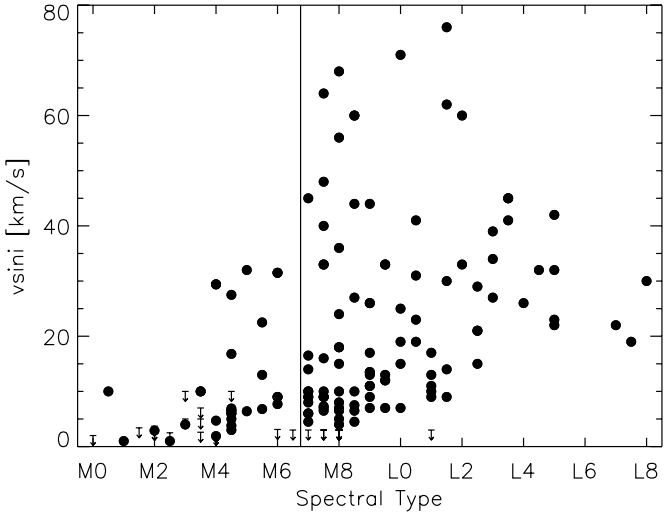

Figure 3. Projected rotation velocities ($v \sin i$) as a function of spectral type for the objects studied in this paper. The region above $v \sin i \approx 30$ km s^{-1} contains no early- or mid-M dwarfs, but is well populated by objects in the range M7–L5.

with SP = 0 for M0 (Wilking et al. 1999); (2) for the L dwarfs we use $BC_K = 3.42 + 0.075(SP - 4)$ for L0–L4 and $BC_K = 3.42 - 0.075(SP - 4)$ for L5–L9, with SP = 0 for L0 (Dahn et al. 2002; Nakajima et al. 2004); and (3) for the T dwarfs we use $BC_K = 3.41 - 0.21(SP)$ with SP = 0 for T0 (Nakajima et al. 2004). We find an overall trend of increasing radio activity with later spectral type, at least to spectral type ∼L4, with a dearth of sources with $L_{rad}/L_{bol} \gtrsim 10^{-7}$ in spectral types earlier than M6 (see also Berger 2002, 2006; Hallinan et al. 2008). Moreover, essentially every detected object beyond a spectral type of M7 exhibits a value of L_{rad}/L_{bol} that is larger than the saturated activity level in the M0–M6 dwarfs.

The distribution of rotation velocities as a function of spectral type is shown in Figure 3. There are no M0–M6 dwarfs with rotation velocities of $v \sin i \gtrsim 30$ km s^{-1}, while among the ultracool dwarfs the sample is fairly uniformly distributed over the range of ≈5–60 km s^{-1}. We note that unavoidably the values of $v \sin i$ include the unknown inclination of the sources. This may lead to increased scatter in activity relations relative to $v \sin i$, but it should not introduce artificial trends, especially since a range of $i = 10°$–$80°$ corresponds to only a factor of about five in $\sin i$. Moreover, the unknown inclinations will have no effect in examining the relative activity trends in the radio, X-rays, and Hα. We also note that even if inclination played a role in the detectability of radio emission (for example, due to non-isotropic emission), the fact that radio emission is detected from objects with a range of a few to tens of km s^{-1} suggests that variations in inclination cannot be the sole reason.

Combining the rotation velocities with the radio luminosities (Figure 4), we find no clear correlation, although there is a tantalizing paucity of objects with $v \sin i \gtrsim 30$ km s^{-1} and radio luminosity of $\lesssim 10^{23}$ erg s^{-1}, which are present at $v \sin i \lesssim 30$ km s^{-1}. The lack of an obvious change in radio luminosity from early-M dwarfs to ultracool dwarfs contrasts with the trends seen in Hα and X-rays (Berger et al. 2010).

Since the X-ray and Hα rotation trends are strongest when scaled relative to the bolometric luminosity, we plot L_{rad}/L_{bol} as a function of rotation velocity in Figure 5. In the early- to mid-M dwarfs, we find an apparent radio rotation–activity relation, with subsequent saturation at $v \sin i \gtrsim 5$ km s^{-1} and $L_{rad}/L_{bol} \approx 10^{-7.5}$. There are few detections below the saturation velocity, but the bulk of the upper limits for the slow rotators are well below the saturated emission level. This behavior is consistent with the rotation–activity relation observed in the X-rays, as expected from the radio/X-ray correlation in early-M dwarfs (Guedel & Benz 1993; Benz & Guedel 1994). It is also similar to the Hα rotation–activity relation (Delfosse et al. 1998; Mohanty & Basri 2003). On the other hand, the detected late-M and L dwarfs exhibit a general increase in L_{rad}/L_{bol} compared to M0–M6 (Figure 2). Therefore, the ultracool dwarfs no longer follow the saturation level observed in the early-M dwarfs, and instead reside at higher values of $L_{rad}/L_{bol} \sim 10^{-6.4}$. There is also an increase in the scatter of radio activity levels in ultracool dwarfs, similar to that seen in X-rays and Hα (see Figure 6). The

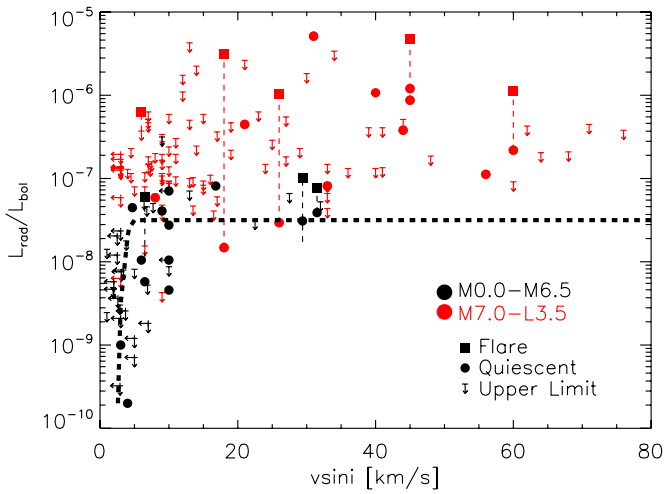

Figure 5. Ratio of radio to bolometric luminosity as a function of projected rotation velocity. Shown are flares (squares), quiescent emission (circles), and radio upper limits (arrows). Left arrows indicate upper limits in $v \sin i$. Red symbols represent objects later than M7, while black symbols represent objects with spectral types M0–M6.5. The early- to mid-M dwarfs appear to reach a saturated level of $L_{\rm rad}/L_{\rm bol} \approx 10^{-7.5}$ at $v \sin i \gtrsim 5$ km^{-1}. The black dashed line indicates a rough fit to the radio activity–rotation relation for objects earlier than M7. There is a general increase in $L_{\rm rad}/L_{\rm bol}$ among the late-M and L dwarfs (as seen in Figure 2), as well as an increase in the scatter. There are also indications of a trend toward higher luminosity ratios in the fastest rotators, $v \sin i \gtrsim 30$ km s^{-1}.

(A color version of this figure is available in the online journal.)

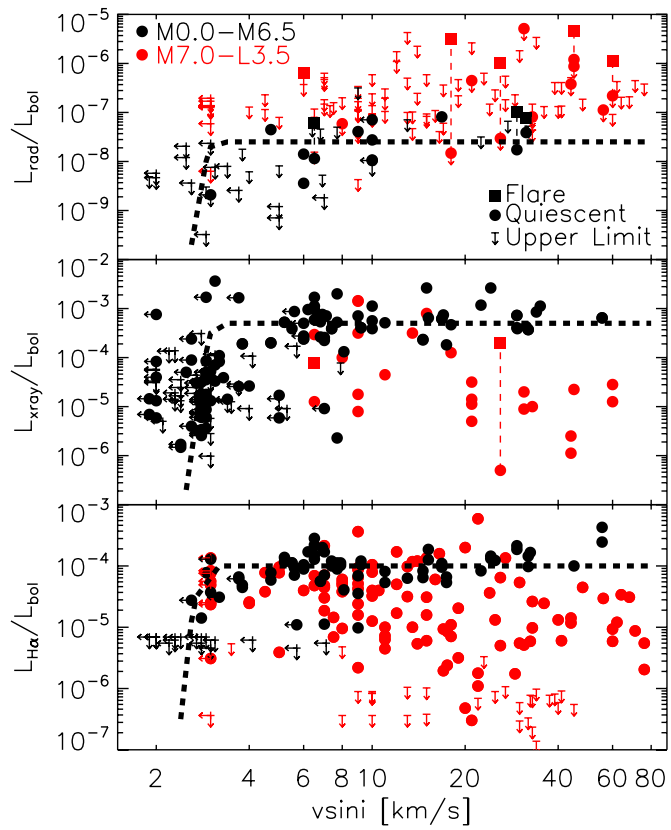

Figure 6. Radio, X-ray, and Hα activity as a function of projected rotation velocity. Shown are flares (squares), quiescent emission (circles), and upper limits (arrows). Left arrows indicate upper limits in $v \sin i$. Red symbols represent objects later than M7, while black symbols represent objects with spectral types M0–M6.5. X-ray data are taken from Berger et al. (2008), James et al. (2000), Delfosse et al. (1998), and Pizzolato et al. (2003). Hα data are taken from Delfosse et al. (1998), Mohanty & Basri (2003), and Reiners & Basri (2008, 2010). All three activity indicators appear to saturate at ~5 km s^{-1} for objects earlier than M6. The Hα and X-ray activity–rotation relations break down at M7–M9 (Berger et al. 2008; Reiners & Basri 2010) with the activity dropping rapidly and the scatter increasing in later spectral types. There are hints of "super-saturation" above ~30 km s^{-1} where the luminosity drops in the most rapidly rotating objects. The radio activity follows a similar trend to the X-ray activity in the earlier objects. However, beyond M7, it begins to exhibit the opposite behavior.

(A color version of this figure is available in the online journal.)

increased scatter is indicative of a breakdown in the correlation between the activity level and rotation velocity. On the other hand, at $v \sin i \gtrsim 20$ km s^{-1}, where the X-ray and Hα activity appear to exhibit super-saturation, there are indications of a trend toward higher radio activity levels (Figure 6). It is therefore clear that the radio activity and the Hα/X-ray trends diverge in ultracool dwarfs, regardless of whether we normalize by the bolometric luminosity or not.

We further explore the role of rotation by investigating the fraction of objects with radio detections as a function of rotation velocity. We divide the objects with spectral types M7–L4 into three $v \sin i$ bins, using two sets of binning, and retaining only significant non-detections, i.e., those with $L_{\rm rad} \lesssim 2.5 \times 10^{23}$ erg s^{-1}, which is the typical luminosity of the detected sources. The results are shown in Figure 7. For both sets of binning we find a clear increase in the fraction of radio detections as a function of $v \sin i$, from a few percent at $v \sin i \lesssim 15$ km s^{-1} to about 30% at $v \sin i \gtrsim 30$ km s^{-1}. This result suggests that while radio luminosity may not increase with faster rotation, the probability of producing radio emission does depend on fast rotation. This may be due to the influence of rotation on the magnetic field strength and/or its topology.

Studies of X-ray, Ca II *H&K*, and Hα activity indicate that the Rossby number is the rotation parameter most highly closely correlated with magnetic activity (Noyes et al. 1984). We estimate the Rossby numbers for our sample using the method of Reiners & Basri (2010). The periods are estimated from $v \sin i$ combined with radii estimated from the mass–magnitude (Delfosse et al. 2000) and mass–radius (Baraffe et al. 1998) relations. A radius of 0.1 $R_\odot$ is used for spectral types beyond M8. We estimate τ_c using the empirical relation of Kiraga & Stepien (2007) imposing a maximum of 70 days, consistent with Gilliland (1986). In Figure 8, we plot radio luminosity as a function of Ro. As in the case of radio luminosity versus $v \sin i$, we find no significant evolution from early-M to ultracool dwarfs. However, we note that the ultracool dwarfs with radio emission are clearly concentrated at Ro $\lesssim 5 \times 10^{-3}$, indicating that objects with low Rossby numbers are more likely to produce detectable radio activity.

In Figure 9, we plot the luminosity in radio, X-ray, and Hα scaled by the bolometric luminosity as a function of Ro. We supplement our data with results for F–K stars from the literature (Mekkaden 1985; Stewart et al. 1988; Slee & Stewart 1989; Delfosse et al. 1998; James et al. 2000; Pizzolato et al. 2003). The previously discussed trends in X-ray and Hα activity versus $v \sin i$ are more pronounced when plotted versus Rossby number. In particular, for spectral types earlier than M6 the X-ray activity exhibits a rapid increase by about three orders of magnitude as Ro decreases from ~2 to ~0.2, followed by saturation at Ro $\lesssim$ 0.2. The ultracool dwarfs exhibit a clear super-saturation trend of decreasing activity as a function of decreasing Rossby number in the range Ro $\approx 10^{-2}$ to 10^{-3} (see also Berger et al. 2008). A similar trend is apparent in Hα activity (see also Reiners & Basri 2010). On the other

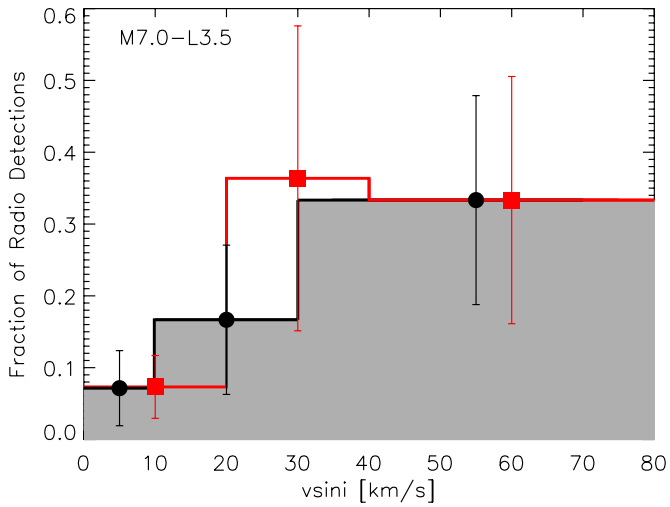

Figure 7. Fraction of objects with radio detections as a function of rotation velocity for ultracool dwarfs with spectral types M7–L4. Upper limits above $L_{\rm rad} \approx 2.5 \times 10^{23}$ erg s^{-1} have been excluded. Uncertainties are determined from the Poisson distribution. Two different sets of binning are shown in order to test the impact of the choice of boundaries. There is a clear increase in the fraction of detected objects among the fastest rotators. The transition seems to occur at $v \sin i \approx$ 20–30 km s^{-1}.

(A color version of this figure is available in the online journal.)

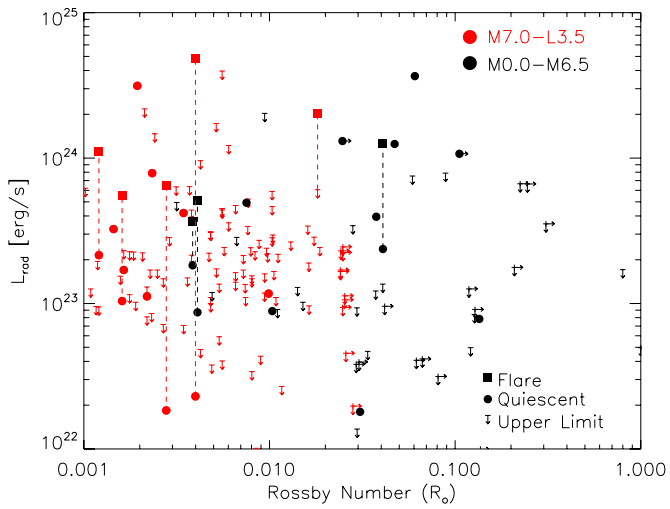

Figure 8. Radio luminosity as a function of Rossby number (Ro $= P/\tau_c$). Shown are flares (squares), quiescent emission (circles), and radio upper limits (arrows). Right arrows indicate lower limits in Ro. Red symbols represent objects later than M7, while black symbols represent objects with spectral types M0–M6.5. As in Figure 4, no correlation between $L_{\rm rad}$ and Ro is obvious, but the bulk of ultracool dwarfs with radio detections are concentrated at low Rossby numbers, Ro $\lesssim 5 \times 10^{-3}$.

(A color version of this figure is available in the online journal.)

hand, in the radio band we find a uniform trend of increasing activity as a function of decreasing Rossby number over the range Ro $\approx$ 0.1–10^{-3} and for spectral types G to L, indicating that at least in some ultracool dwarfs, there is no evidence for a breakdown in the activity–Rossby-number relation. A Spearman's rank correlation test for the detected sources gives $\rho \approx -0.88$ with a null hypothesis (no correlation) probability of only $\approx 1.1 \times 10^{-15}$. A linear regression fit indicates an overall trend of $L_{\rm rad}/L_{\rm bol} \propto {\rm Ro}^{-1.1}$.

Finally, Slee & Stewart (1989) noted the potential importance of radio surface flux ($L_{\rm rad}/R_*^2$) as a quantity strongly correlated with rotation in G–K stars; here R_* is the stellar radius

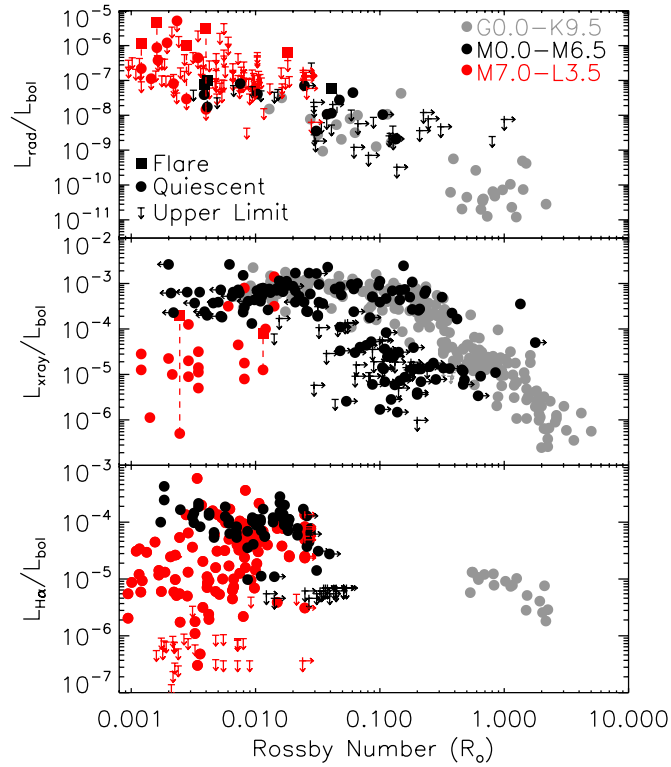

Figure 9. Radio, X-ray, and Hα activity as a function of Rossby number. Shown are flares (squares), quiescent emission (circles), and upper limits (arrows). Right arrows indicate lower limits in Ro. Red symbols represent objects later than M7, black symbols represent objects with spectral types M0–M6.5, and gray symbols represent spectral types G–K. X-ray data are from James et al. (2000), Delfosse et al. (1998), Pizzolato et al. (2003), and Berger et al. (2008). Hα data are from Mekkaden (1985), Delfosse et al. (1998), Mohanty & Basri (2003), and Reiners & Basri (2008, 2010). Radio data for the G–K stars are from Stewart et al. (1988), Slee & Stewart (1989), and Guedel et al. (1995). As in Figure 6, the Hα and X-ray activity–rotation relations break down at M7–M9 (Berger et al. 2008; Reiners & Basri 2010), with the activity dropping rapidly and the scatter increasing in later spectral types. There are hints of "super-saturation" in the most rapidly rotating ultracool dwarfs with Ro $\lesssim$ 0.01. The radio activity appears to follow a single trend with Rossby number from M0–L4 and Ro $\approx$ 0.1–10^{-3}.

(A color version of this figure is available in the online journal.)

normalized to solar units. These authors found that $L_{\rm rad}/R_*^2 \propto P^{-1.8\pm0.3}\, R_*^{1.8\pm0.4}$. In Figure 10, we plot radio surface flux as a function of Rossby number for the ultracool dwarfs in our sample and from the literature, as well as for the main-sequence stars in the Slee & Stewart (1989) sample. The objects, ranging from spectral type G to L, again appear to follow a single trend with respect to Ro. A Spearman's rank correlation test for the detected sources gives $\rho \approx -0.72$ with a null hypothesis (no correlation) probability of only $\approx 7.0 \times 10^{-8}$. A linear regression fit indicates an overall trend of $L_{\rm rad}/R_*^2 \propto {\rm Ro}^{-0.5}$.

5. IMPLICATIONS FOR MAGNETIC DYNAMO MODELS

The single trend of radio activity and surface flux as a function of Rossby number for G–L dwarfs, the overall increase in radio activity with rotation velocity, and the enhanced fraction of radio emitters at $v \sin i \gtrsim 25$ km s^{-1} indicate that rotation continues to play a role in the dynamo mechanism of ultracool dwarfs. These trends are at odds with observations in X-rays and Hα, which point to a breakdown in the relation between activity and rotation. This suggests that the reduced activity levels in X-rays and Hα are due to external effects, such as

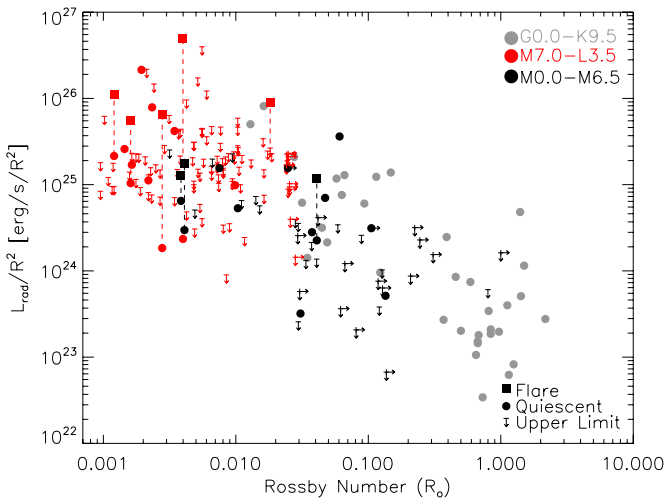

Figure 10. Radio surface flux as a function of Rossby number. Shown are flares (squares), quiescent emission (circles), and upper limits (arrows). Right arrows indicate lower limits in Ro. Red symbols represent objects later than M7, black symbols represent objects with spectral types M0–M6.5, and gray symbols represent spectral types G–K (Stewart et al. 1988; Slee & Stewart 1989; Guedel et al. 1995). The stellar radii are in units of $R_\odot$. As in the case of L_{rad}/L_{bol}, the surface flux appears to follow a single trend from spectral types G2 to L4. The overall trend is roughly linear, $L_{rad}/R_*^2 \propto \mathrm{Ro}^{-1}$.

(A color version of this figure is available in the online journal.)

the increased neutrality of the atmospheres, a reduction in the efficiency of bulk coronal heating, or centrifugal stripping, rather than to a substantial decrease in the dynamo efficiency. In this context, the radio observations provide strong support to Zeeman measurements that point to the continued presence of ∼1–3 kG fields in some late-M dwarfs (Morin et al. 2010; Reiners & Basri 2010). However, ZDI measurements suggest a breakdown in the correlation between stellar parameters (e.g., rotation) and the field strength for Ro $\lesssim$ 0.1 such that some rapid rotators have weak fields, while others have substantial fields (Morin et al. 2010). The evidence from radio observations extends to faster rotation velocities than the limit of $v \sin i \lesssim$ 20 km s^{-1} for Zeeman measurements, and may be indicative of a similar trend: namely rapid rotators are more likely to produce radio emission, and to follow the same trend with respect to Rossby number of G–K stars, but there is a large fraction of rapid rotators with no detectable radio emission.

With the exception of the purely turbulent dynamo model of Durney et al. (1993), all other published models of fully convective dynamos predict some level of relation between the magnetic energy density and rotation, at least up to a saturation level (Chabrier & Küker 2006; Dobler et al. 2006; Browning 2008). In particular, Chabrier & Küker (2006) find that in an α^2 dynamo the resulting field strength depends on rotation up to a saturation value, and it may indeed dominate in the fastest rotators leading to the activity–rotation saturation observed in X-rays and Hα. Similarly, Dobler et al. (2006) find that on large scales the magnetic energy increases with rotation (up to some saturation value), while small-scale fields are nearly independent of rotation. Browning (2008) also finds that faster rotators produce stronger fields and that rapid rotation leads to suppression of differential rotation.

The dynamo models also predict that rotation will affect the field topology, but there is little agreement about the resulting field configurations. Predictions range from dominant axisymmetric fields (Browning 2008), with a primary quadrupolar component (Dobler et al. 2006), to large-scale, non-axisymmetric, high multipole order fields (Chabrier & Küker 2006). As in the case of field strength, field topology measurements with the ZDI technique suggest that in late-M dwarfs there is no clear correlation between stellar parameters (e.g., rotation) and the field topology. Since a substantial fraction of the radio emitters produce simple rotationally modulated emission indicative of a dipolar field topology (Berger et al. 2005, 2009; Hallinan et al. 2006, 2007; McLean et al. 2011), it is possible that magnetic topology rather than field strength is the key to the change in the nature of magnetic activity among ultracool dwarfs, and that this is the main parameter that is correlated with rotation. A clear test of this possibility is to observe all radio emitters for at least a few rotation periods to test for periodicity. For the objects with $v \sin i \lesssim$ 20 km s^{-1} this will require ∼40 hr per source.

6. CONCLUSIONS

We presented new observations of a large sample of M and L dwarfs with measured rotation velocities aimed at addressing the radio activity–rotation relation in fully convective objects. This survey triples the number of ultracool dwarfs with measured rotation velocities and radio observations. As part of this survey we also discovered three new radio active ultracool dwarfs, of which one (2M1314+1320) exhibits periodic radio emission (McLean et al. 2011). Combining our observations with objects from the literature we find the following key results.

1. In the M0–M6 dwarfs we find a saturation-type relation between rotation period and radio activity, similar to the one seen in Hα and X-ray, and reaching saturation at a relatively low rotation velocity of about 5 km s^{-1}.
2. Unlike the rapid decline in X-ray and Hα activity in ultracool dwarfs, even for the most rapid rotators, the radio luminosity remains unchanged as a function of rotation velocity and spectral type, at least to spectral type of about L4. The ratio of radio to bolometric luminosity increases with later spectral type, well beyond the saturation value of M0–M6 dwarfs. However, as in the case of X-ray and Hα activity we find an increased scatter in L_{rad} and L_{rad}/L_{bol} for ultracool dwarfs.
3. In the regime of fastest rotation ($v \sin i \gtrsim$ 20 km s^{-1}), there are fewer objects with low radio luminosity and a higher fraction of detected objects. This is contrary to the apparent X-ray and Hα super-saturation in these fast rotators.
4. The ratio of radio to bolometric luminosity and the radio surface flux increase as a function of decreasing Rossby number with a single trend for Ro ∼ 0.1–10^{-3} and spectral types G–L. This is in direct contrast to the saturated X-ray/Hα activity–Ro relation in G–L dwarfs, and the X-ray/Hα super-saturation in ultracool dwarfs.

Our most basic conclusion from these observations is that rotation continues to play a role in the magnetic activity of ultracool dwarfs, and hence in the underlying dynamo mechanism. It is not possible at the present to determine whether rotation mainly influences the field strength or its topology, since both may affect the detectability of radio emission. A clear test is long-term monitoring of the radio emitters to check for periodic modulation, which will allow us to reconstruct the field configuration (Berger et al. 2009; McLean et al. 2011). The ability of radio observations to trace the presence of magnetic fields in the most rapid rotators ($v \sin i \gtrsim$ 20 km s^{-1}) is particularly important in light of the inability of Zeeman measurements to probe this regime. We are clearly able to study the role of rotation down to Ro ∼ 10^{-3}, while the Zeeman

techniques are sensitive only to Ro $\gtrsim 10^{-2}$ (Morin et al. 2010; Reiners & Basri 2010).

While rotation clearly plays a role in radio activity, there are rapid rotators with no detectable radio emission, suggesting that more than one dynamo mechanism could be operating in ultracool dwarfs or that the dynamo may lead to significantly different strengths/topologies. This is similar to the conclusion of Morin et al. (2010) from ZDI measurements of mid- and late-M dwarfs. In particular, it is possible that some rapid rotators are dominated by a dynamo that leads to a large-scale, low multipole order field that is more likely to result in detectable radio emission (particularly simple periodic radio emission). The long-term variability of at least some ultracool dwarfs (Section 3; Antonova et al. 2008; Berger et al. 2010) may be indicative of an episodic switch between the dynamo states.

Since most of the radio detections of ultracool dwarfs to date are close to the sensitivity limit of the VLA, future studies of individual objects and trends such as the activity–rotation relation will greatly benefit from the order-of-magnitude increase in sensitivity afforded by the now-operational Expanded Very Large Array. Any constraints on the convective dynamo mechanism, atmospheric coupling of the magnetic field, or bulk coronal densities must take results from radio activity studies into account, particularly for the fastest rotators. In addition, theoretical dynamo models should explore the range of stellar parameters and rotation rates that are directly probed by radio observations, extending down to at least Ro $\sim 10^{-3}$.

E.B. acknowledges support for this work from the National Science Foundation through Grant AST-1008361. A.R. received research funding from the DFG as an Emmy Noether Fellow (RE 1664/4-1). This work has made use of the SIMBAD database, operated at CDS, Strasbourg, France.

REFERENCES

Antonova, A., Doyle, J. G., Hallinan, G., Bourke, S., & Golden, A. 2008, A&A, 487, 317
Baraffe, I., Chabrier, G., Allard, F., & Hauschildt, P. H. 1998, A&A, 337, 403
Basri, G., & Marcy, G. W. 1995, AJ, 109, 762
Benz, A. O., & Guedel, M. 1994, A&A, 285, 621
Berger, E. 2002, ApJ, 572, 503
Berger, E. 2006, ApJ, 648, 629
Berger, E., Ball, S., Becker, K. M., et al. 2001, Nature, 410, 338
Berger, E., Basri, G., Fleming, T. A., et al. 2010, ApJ, 709, 332
Berger, E., Basri, G., Gizis, J. E., et al. 2008, ApJ, 676, 1307
Berger, E., Rutledge, R. E., Phan-Bao, N., et al. 2009, ApJ, 695, 310
Berger, E., Rutledge, R. E., Reid, I. N., et al. 2005, ApJ, 627, 960
Bower, G. C., Bolatto, A., Ford, E. B., & Kalas, P. 2009, ApJ, 701, 1922
Browning, M. K. 2008, ApJ, 676, 1262
Browning, M. K., Basri, G., Marcy, G. W., West, A. A., & Zhang, J. 2010, AJ, 139, 504
Burgasser, A. J., & Putman, M. E. 2005, ApJ, 626, 486
Caillault, J.-P., Drake, S., & Florkowski, D. 1988, AJ, 95, 887
Chabrier, G., & Küker, M. 2006, A&A, 446, 1027
Cruz, K. L., Reid, I. N., Liebert, J., Kirkpatrick, J. D., & Lowrance, P. J. 2003, AJ, 126, 2421
Dahn, C. C., Harris, H. C., Vrba, F. J., et al. 2002, AJ, 124, 1170
Delfosse, X., Forveille, T., Perrier, C., & Mayor, M. 1998, A&A, 331, 581
Delfosse, X., Forveille, T., Ségransan, D., et al. 2000, A&A, 364, 217
Dobler, W., Stix, M., & Brandenburg, A. 2006, ApJ, 638, 336
Donati, J.-F., Forveille, T., Collier Cameron, A., et al. 2006, Science, 311, 633
Durney, B. R., De Young, D. S., & Roxburgh, I. W. 1993, Sol. Phys., 145, 207
Faherty, J. K., Burgasser, A. J., Cruz, K. L., et al. 2009, AJ, 137, 1
Gilliland, R. L. 1986, ApJ, 300, 339
Güdel, M. 2002, ARA&A, 40, 217
Guedel, M., & Benz, A. O. 1993, ApJ, 405, L63
Guedel, M., Schmitt, J. H. M. M., & Benz, A. O. 1995, A&A, 302, 775
Gudel, M., Schmitt, J. H. M. M., Bookbinder, J. A., & Fleming, T. A. 1993, ApJ, 415, 236
Hallinan, G., Antonova, A., Doyle, J. G., et al. 2006, ApJ, 653, 690
Hallinan, G., Antonova, A., Doyle, J. G., et al. 2008, ApJ, 684, 644
Hallinan, G., Bourke, S., Lane, C., et al. 2007, ApJ, 663, L25
Jackson, P. D., Kundu, M. R., & White, S. M. 1989, A&A, 210, 284
James, D. J., Jardine, M. M., Jeffries, R. D., et al. 2000, MNRAS, 318, 1217
Jardine, M., & Unruh, Y. C. 1999, A&A, 346, 883
Jenkins, J. S., Ramsey, L. W., Jones, H. R. A., et al. 2009, ApJ, 704, 975
Kiraga, M., & Stepien, K. 2007, Acta Astron., 57, 149
Krishnamurthi, A., Leto, G., & Linsky, J. L. 1999, AJ, 118, 1369
McLean, M., Berger, E., Irwin, J., Forbrich, J., & Reiners, A. 2011, ApJ, 741, 27
Mekkaden, M. V. 1985, Ap&SS, 117, 381
Mohanty, S., & Basri, G. 2003, ApJ, 583, 451
Mohanty, S., Basri, G., Shu, F., Allard, F., & Chabrier, G. 2002, ApJ, 571, 469
Morin, J., Donati, J.-F., Petit, P., et al. 2010, MNRAS, 407, 2269
Nakajima, T., Tsuji, T., & Yanagisawa, K. 2004, ApJ, 607, 499
Noyes, R. W., Hartmann, L. W., Baliunas, S. L., Duncan, D. K., & Vaughan, A. H. 1984, ApJ, 279, 763
Parker, E. N. 1955, ApJ, 122, 293
Phan-Bao, N., Osten, R. A., Lim, J., Martín, E. L., & Ho, P. T. P. 2007, ApJ, 658, 553
Pizzolato, N., Maggio, A., Micela, G., Sciortino, S., & Ventura, P. 2003, A&A, 397, 147
Ravi, V., Hallinan, G., Hobbs, G., & Champion, D. J. 2011, ApJ, 735, L2
Reid, I. N., Kirkpatrick, J. D., Liebert, J., et al. 2002, AJ, 124, 519
Reiners, A., & Basri, G. 2008, ApJ, 684, 1390
Reiners, A., & Basri, G. 2010, ApJ, 710, 924
Reiners, A., Basri, G., & Browning, M. 2009, ApJ, 692, 538
Slee, O. B., & Stewart, R. T. 1989, MNRAS, 236, 129
Stewart, R. T., Innis, J. L., Slee, O. B., Nelson, G. J., & Wright, A. E. 1988, AJ, 96, 371
White, S. M., Jackson, P. D., & Kundu, M. R. 1989, ApJS, 71, 895
Wilking, B. A., Greene, T. P., & Meyer, M. R. 1999, AJ, 117, 469
Willson, R. F., Lang, K. R., & Foster, P. 1988, A&A, 199, 255